PROCEEDINGS OF SCIENCE

Cross-counter time-delay distributions at the Mawson neutron monitor

Alejandro Sáiz,[a,*] **David Ruffolo,**[a] **Thanakorn Sukha,**[a] **Pradiphat Muangha,**[a] **Warit Mitthumsiri,**[a] **Kullapha Chaiwongkhot,**[a] **Waraporn Nuntiyakul,**[b] **Ekkarach Somboon,**[b] **Paul Evenson,**[c] **Marc Duldig**[d] **and John Humble**[d]

[a] *Department of Physics, Faculty of Science, Mahidol University, Bangkok 10400, Thailand*

[b] *Department of Physics and Materials Science, Faculty of Science, Chiang Mai University, Chiang Mai 50200, Thailand*

[c] *Department of Physics and Astronomy, University of Delaware, Newark, DE 19716, USA*

[d] *School of Natural Sciences, University of Tasmania, Hobart, Tasmania 7001, Australia*

E-mail: alejandro.sai@mahidol.ac.th

For decades, neutron monitors have been the primary source of ground-level data for studying cosmic rays with rigidities slightly above the geomagnetic cutoff. The NM64 instrument design, the standard for neutron monitors, has been optimized to monitor neutrons produced in atmospheric cascades. It includes thick slabs of polyethylene to reflect low-energy neutrons, a large mass of Pb to multiply signals at high energies, and an array of cylindrical, gas-filled proportional neutron counters. Mawson station, located in the Australian Antarctic Territory, has one of the longest continually operated polar monitors. In 2020, the station's neutron monitor was upgraded to allow the recording of timing information for individual signal pulses. Also at that time, an extra array of 6 bare counters (with no Pb or polyethylene reflector) was installed in addition to the 3 standard sections of 6 counters each. We analyze the cross-counter time-delay distributions to study timing correlations between pulses on different counters. The results show the expected dependence with tube separation within each NM64 section and clear correlations between different sections and between NM64 and bare counters, which can be at relative distances of up to 10 meters. The cross-counter time-delay distributions may thus be used to study the structure and size of atmospheric cascades. The timing information recorded by the upgraded monitor provides a new dimension of data for researchers to analyze and gain insight into the complex processes of cosmic ray propagation and interaction with Earth's atmosphere.

38th International Cosmic Ray Conference (ICRC2023)
26 July - 3 August, 2023
Nagoya, Japan

*Speaker

PoS(ICRC2023)1351

1. Introduction

Neutron monitors are large (order $\sim$ 10 m^2) ground-based instruments designed to indirectly measure the flux of cosmic rays in space by recording the rate of atmospheric secondary particles (mostly neutrons) produced in atmospheric cascades that reach ground level. The standard NM64 uses $^{10}BF_3$ (or ^{3}He) gas-filled, cylindrical proportional counters inside a big mass of Pb surrounded by thick slabs of polyethylene reflector. In its normal operation, a neutron monitor counts the number of neutron capture events by ^{10}B in each counter; the signal for higher energy neutrons is enhanced by neutron production in the Pb, while the polyethylene reflector prevents environmental neutrons from being recorded (and produced neutrons from escaping). By use of a more modern data acquisition system, times between consecutive neutron captures can be recorded as well, which can be used to infer statistically the energy distribution of atmospheric cosmic rays, since neutrons produced in the Pb by higher energy particles are detected in rapid succession while uncorrelated particles produce more random, Poisson-like time delays. One estimator of cosmic ray energy that uses this approach is the leader fraction [1]. Leader fractions have successfully been used to study solar modulation [2] and tested at different geomagnetic cutoff during latitude surveys [3], and are a promising candidate for a cosmic ray spectral index proxy.

A more recent development in the acquisition system allows us to also record the time between a neutron capture event in one proportional counter and the next event in a different counter, by carefully synchronizing the independent measurements to a common absolute time. Distributions of cross-counter time delays can then be used in the same manner to calculate cross-counter leader fractions, which are useful for gaining insight into the part of the multiplicity signal that does not come from neutron production in the Pb but from the arrival of multiple secondary particles produced in the atmosphere by the same primary cosmic ray [4, 5]. In this work, we present results of cross-counter leader fractions from the neutron monitor at Mawson, Australian Antarctic Territory.

The CosRay Laboratory at Mawson is the oldest continuosly-operated cosmic ray experiment within the Polar Circle. Apart from several muon telescope arrays, it contains a neutron monitor with 3 sections of 6 proportional counters each in the NM64 configuration. In early 2020, two members of our group travelled to Mawson and performed an upgrade in the electronics system and computer software that allows the recording of time delays, both for same-counter and cross-counter combinations. An additional group of 6 counters was also set up in the Laboratory outside of Pb and polyethylene reflector (each only surrounded by a thinner polyethylene moderator), which can be termed bare counters. Although more sensitive to the environment, the radically different energy response of bare counters makes them another valuable tool for cosmic ray energy estimations.

2. Methods

2.1 Cross-counter time-delay histograms

The configuration of NM counters inside the Mawson CosRay Laboratory is shown schematically in Fig. 1. The different segments, including 3 6NM64 sections and an array of bare counters, are distributed along a space $\sim$14 m long, divided by a steel-panel wall. Absolute timing data are available for the 18 counters in NM64 sections and 3 of the bare counters.

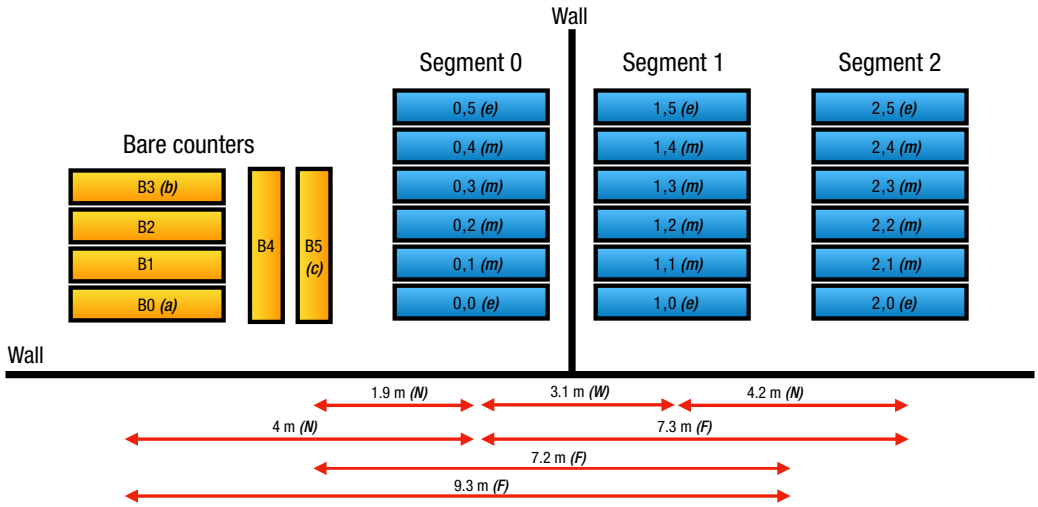

Figure 1: Configuration of the 24 proportional counters at the CosRay Laboratory in Mawson Station. Each rectangle represents a cylindrical counter either as part of a 6NM64 segment (blue) or as a bare counter (yellow). Approximate center-to-center distances between relevant counters or groups of counters are indicated.

Time intervals between a pulse in counter i and the following pulse in counter j are accumulated in histograms that are recorded hourly. Instead of the more than 400 histograms required for acquiring each of the (i, j) combinations separately, we define a matrix, shown in Fig. 2, that assigns a given combination to one of 50 histograms defined as follows: a histogram labelled xRy contains every combination (i, j) in which counter i is of type x, counter j is of type y, and the relative position of the counters is of type R. We categorize the counters by their position relative to the mass of Pb, since this significantly affects their efficiency: if a counter is the left-most or right-most of a 6NM64 section ('end' counter), it is of type e; any of the other four counters of a 6NM64 section ('middle' counter) is called type m; bare counters are also a distinct type, but since they are much more sensitive to the surroundings and the 3 counters used for this analysis are situated at different distances, we record each separately and here label them a, b, and c. The relative position R within one 6NM64 section is simply the counter separation $\Delta = |i - j|$. For cross-segment histograms, R is defined as N if the segments are at a distance less than 5 m and on the same side of the wall ('near'), F if they are at larger distances ('far'), and W if they are not far but on opposite sides of the wall.

2.2 Calculation of cross-counter leader fractions

All 50 hourly time-delay histograms are processed in a similar way as described in previous work [1, 2, 4, 5]: an exponential function is used to fit the histograms in the range (5, 500) ms and the fit parameters are used to construct a leader fraction L for each histogram: the ratio of pulses in the exponential over total pulses in the histogram. Both numerator and denominator are

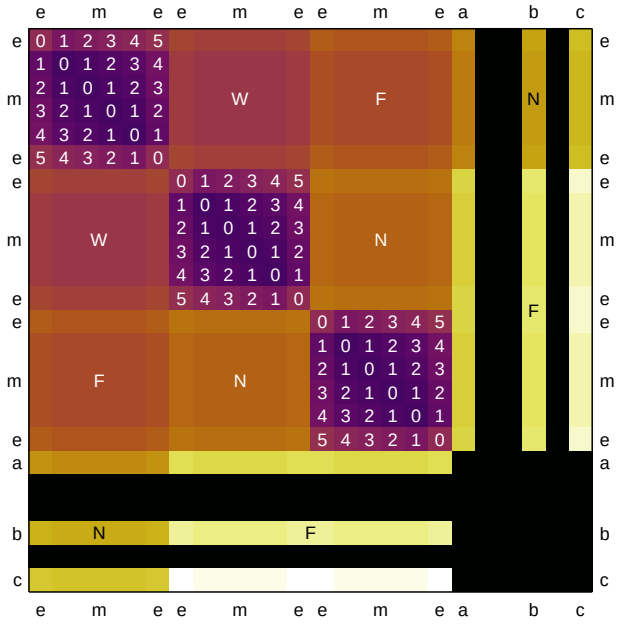

Figure 2: Matrix specifying how a combination (i, j) is assigned to a histogram xRy. Different histograms are represented by different colors. Each row number i runs along the total number of counters (ordered as: counters of Segment 0, Segment 1, Segment 2, bares) and belongs to type x (e, m, a, b, or c) as indicated on the edge. Similarly for each column number j and type y. The relative position types R ($0, \ldots, 5$, W, N, or F) are indicated in the corresponding matrix blocks. Black cells mean those combinations are not recorded.

extrapolated to $t \to \infty$ from $t_{\max} = 500$ ms using the fit parameters A and α:

$$L = \frac{\int_0^\infty A\mathrm{e}^{-\alpha t}\,\mathrm{d}t}{\int_0^\infty n_{\mathrm{data}}(t)\,\mathrm{d}t} \equiv \frac{A/\alpha}{\int_0^{t_{\max}} n_{\mathrm{data}}(t)\,\mathrm{d}t + (A/\alpha)\mathrm{e}^{-\alpha t_{\max}}}$$

If the accumulated histogram in the denominator starts at a value other than zero, say, t_{d}, due to the electronics dead time, the numerator is changed accordingly by multiplying it by $\mathrm{e}^{-\alpha t_{\mathrm{d}}}$. In our case, the dead time is only noticeable for same-counter histograms, i.e., $R = |i - j| = 0$, which are only $m0m$ and $e0e$, for which we apply this small correction ($t_{\mathrm{d}} \sim 0.1$ ms and $\mathrm{e}^{-\alpha t_{\mathrm{d}}} \sim 0.9999$).

2.3 Corrections

Hourly values for the 50 cross-counter leader fractions L_{xRy} are shown in Fig. 3 for the first year of operation and the most recent 9 months. Apart from sporadic noise due to incomplete histogram recording or poor fits (and long periods of unusable data during 2021–2022, not shown), several modifications to the system were applied during this interval of time (in most cases, with the objective of improving the absolute timing estimation), including the discontinuation of specific counters, changes in the data acquisition software, and tuning of the electronics, which had an effect on some of the L_{xRy} values; however, the qualitative properties of these data can be assumed to be unchanged.

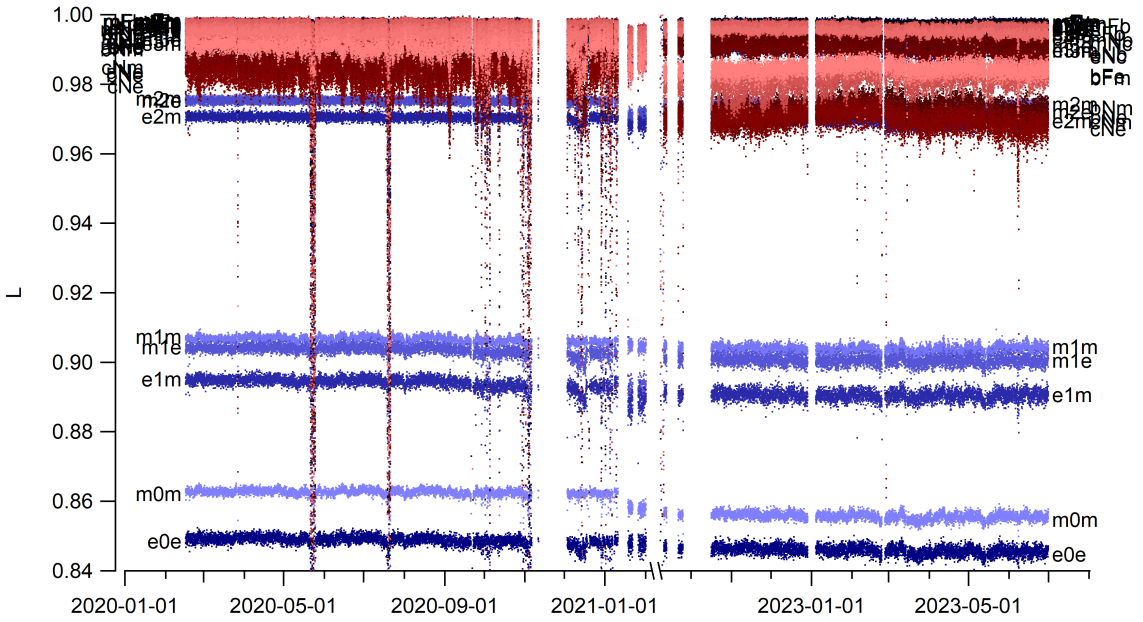

Figure 3: Cross-counter leader fractions L for all histograms xRy calculated hourly, before any correction.

Data cleaning and pressure correction were applied to the L_{xRy} data separately for each time period during which there was no substantial system modifications. Histograms with unusually low number of pulses or resulting in substandard exponential fits (in terms of χ^2 values or estimated parameter errors) were discarded. The remaining values of L_{xRy} show small but clear correlations with atmospheric pressure p, due to the inherent connection between our data and the size and structure of cosmic ray atmospheric cascades. Each L_{xRy} is thus corrected by a multiplicative factor $\exp[-b(p - p_0)]$ to a reference pressure p_0 using a pressure correction coefficient b calculated as the slope of a fit to the deviations of $\log L$ vs. the deviations of p with respect to their moving averages (using a 15-day window). Besides this, no other correction for environmental effects was attempted.

3. Results and Discussion

3.1 Corrected leader fractions

Corrected values of L_{xRy} are presented in Fig. 4. Most time variations during stable intervals are insignificant. Here we choose the time period before the first system modification (2020 Feb. 16–Sep. 21) to exemplify the dependence of L_{xRy} with distance and type of counters. We plot median values during this time period in Fig. 5.

As observed previously in the Princess Sirindhorn neutron monitor (PSNM) in Thailand [5], leader fractions L_{xRy} involving only counters in the same NM64 section ($x, y = e$ or m, $R = |i - j|$) depend strongly on counter separation due to the lateral propagation of neutrons produced in the Pb from a common atmospheric secondary cosmic ray, getting closer to 1 for distant counter

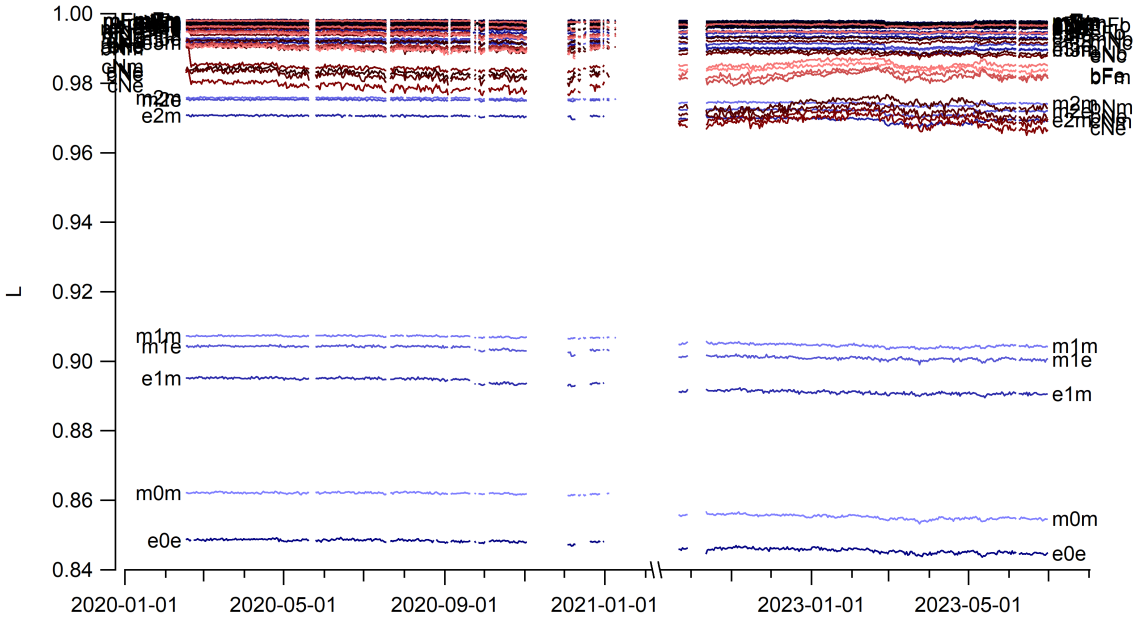

Figure 4: Cross-counter leader fractions L for all histograms xRy averaged daily, after cleaning and pressure correction.

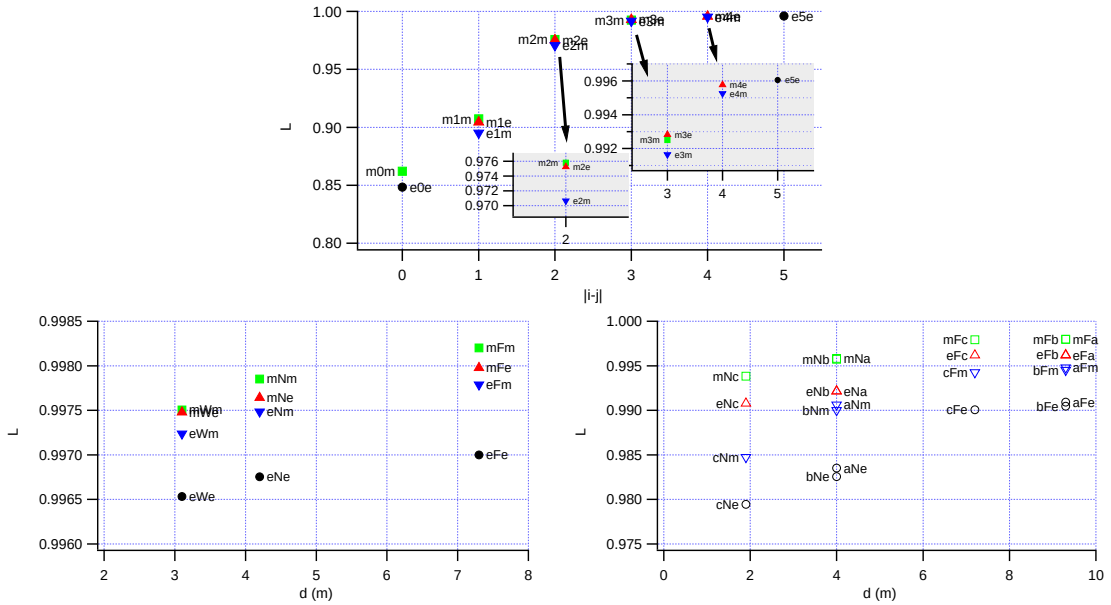

Figure 5: Top panel: median values of L_{xRy} for same-segment combinations of NM64 counters as a function of counter separation $|i-j|$. Bottom: median L_{xRy} as a function of distance for (left) cross-segment combinations of NM64 counters and (right) bare-NM64 combinations. Different symbols represent different (x, y) pairs.

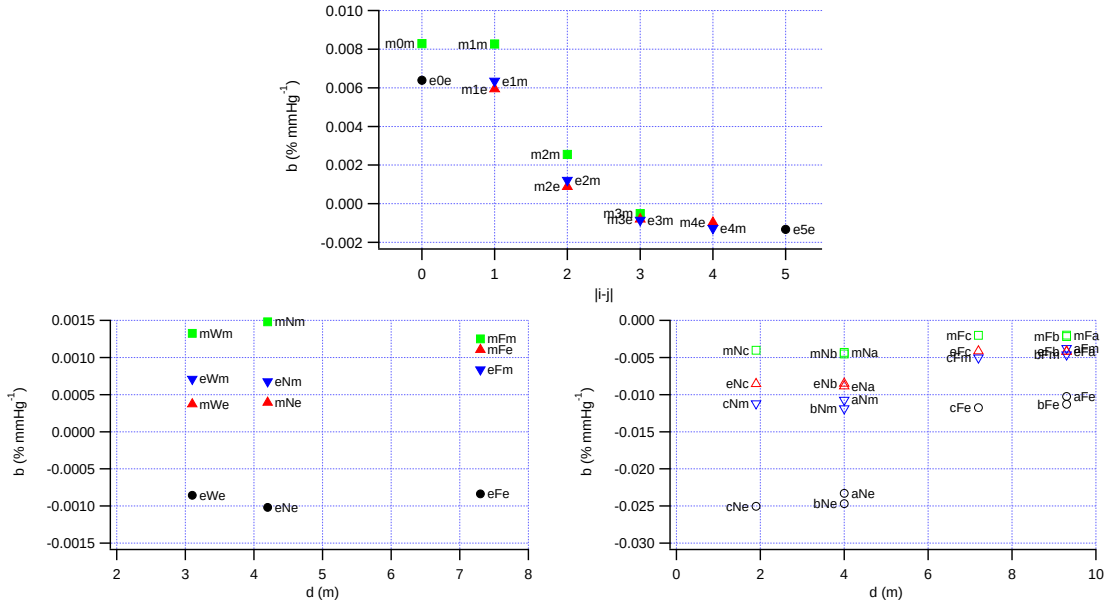

Figure 6: Same as Fig. 5 for the atmospheric pressure correction coefficients b.

combinations. The effect of counter position relative to the mass of Pb is also visible, related to the lower efficiency of e counters.

For the cases involving two different NM64 sections ($x, y = e$ or m, $R = W$, N, or F), dependence on distance is still strong, but the values of L_{xRy} seem to approach a limit not consistent with 1 (perfect exponential), which can be explained as simultaneous measurement of multiple secondary cosmic rays produced by the same primary. Dependence on counter type does not match the trends at PSNM (situated at high geomagnetic cutoff and high altitude), for which the me and ee combinations at a distance of 8 m are higher (~0.9975) than the mm and em (~0.9969) [5]. Note that tube separation $|i - j|$ in one segment can be expressed as distance between counters d by $d \sim (0.5\text{ m}) \times |i - j|$ for comparison purposes.

When one of the counters is a bare (x or $y = a$, b, or c), relative distance also plays a major role, with xRa and xRb giving virtually identical values of L (counters a and b are roughly at the same distance to a given 6NM64 section) and aRy giving L slightly higher than bRy due to the higher efficiency (~ 5%) of bare a compared to b. For $R = F$ combinations, all three bares a, b, c produce very consistent values of L for a given combination with the other x or y, suggesting that the presence of a wall between the bares and the 6NM64 sections has more relevance than distance alone.

3.2 Pressure coefficients

Fig. 6 shows the values of coefficients b for the same time period as above (2020 Feb. 16–Sep. 21). Although small ($|b| < 0.015\%\,\text{mmHg}^{-1}$ in most cases), they show clear patterns with respect to counter separation and counter types, and vary from positive values consistent with what was found previously for the same-counter leader fraction [1] to negative values for some xRy. We do not have an explanation for this at the moment.

4. Conclusions

We have analyzed the 50 cross-counter time-delay histograms arising from combinations of interest between different proportional counters in the Mawson neutron monitor. Its configuration in disjoint sections of 6NM64 at different distances, plus the inclusion of bare counters in the system, provide unique oportunities to study the extent and properties of cosmic ray showers, once we take into account the subtleties introduced by the varied counter efficiencies.

Acknowledgments

We thank the Australian Antarctic Division for their continuous support of scientific activities at Mawson. We are also indebted to the Bureau of Meterology of Australia for technical assistance. Work in Thailand was supported by the National Science and Technology Development Agency (NSTDA) and the National Research Council of Thailand (NRCT) under the High-Potential Research Team Grant Program (N42A650868), and from the NSRF via the Program Management Unit for Human Resources & Institutional Development, Research and Innovation (B37G660015).

References

[1] D. Ruffolo, A. Sáiz, P.-S. Mangeard, N. Kamyan, P. Muangha, T. Nutaro et al., *Monitoring short-term cosmic-ray spectral variations using neutron monitor time-delay measurements*, *Astrophys. J.* **817** (2016) 38.

[2] C. Banglieng, H. Janthaloet, D. Ruffolo, A. Sáiz, W. Mitthumsiri, P. Muangha et al., *Tracking cosmic-ray spectral variation during 2007–2018 using neutron monitor time-delay measurements*, *Astrophys. J.* **890** (2020) 21.

[3] P.-S. Mangeard, D. Ruffolo, A. Sáiz, W. Nuntiyakul, J.W. Bieber, J. Clem et al., *Dependence of the neutron monitor count rate and time delay distribution on the rigidity spectrum of primary cosmic rays*, *J. Geophys. Res.: Space Phys.* **121** (2016) 11,620.

[4] A. Sáiz, W. Mitthumsiri, D. Ruffolo, P. Evenson and T. Nutaro, *Measurement of cross-counter leader fractions in an 18NM64: Detecting single and multiple atmospheric secondaries*, *PoS* **ICRC2017** (2017) 047.

[5] A. Sáiz, W. Mitthumsiri, D. Ruffolo, P. Evenson and T. Nutaro, *Detecting single and multiple atmospheric secondaries in an 18NM64*, *PoS* **ICRC2019** (2019) 1145.